A Novel Proportional Resonant Observer Based Digital Control Strategy For 400Hz Ground Power Unit

Son Tran Que[1], Linh Nguyen Ba[2], Huynh Van Diep[2], Cao Viet Long[2], Nguyen Quang Dich[1], and Nguyen Kien Trung[2*]

[1] *Institute for Control Engineering and Automation, Hanoi University of Science and Technology, Vietnam*
[2] *School of Electrical and Electronic Engineering, Hanoi University of Science and Technology, Vietnam*
[*] *Corresponding author. E-mail: trung.nguyenkien1@hust.edu.vn*

Received: Nov. 01, 2023; Accepted: Apr. 18, 2024

This paper studies a novel Proportional Resonant (PR) disturbance observer (PRobs) design for a 400Hz frequency converter Ground Power Unit (GPU), a device that provides electrical power to aircrafts while they are on the ground. The observer is proposed to estimate the output voltage and inductor current, as well as the unmeasurable system disturbances resulting from system parameter variations and load changes. The PR control algorithm, designed to achieve a high gain at resonant frequency, is employed to minimize the estimation error between the estimated and actual states, thereby providing highly accurate estimated values for voltage, current, and system disturbances. A single loop control strategy based on the observer's estimated output is implemented to regulate the inverter's output voltage. The system demonstrates strong robustness as disturbances can be estimated and cancelled out. Matlab simulations are initially conducted, followed by real-time simulations using a hardware-in-the-loop (HIL) setup to validate the method's effectiveness. Finally, the design is verified through experimental testing.

Keywords: Ground power unit, PR observer, disturbance estimation, single loop controller

http://dx.doi.org/10.6180/jase.202503_28(3).0009

1. Introduction

GPU is the device which powers the airplane during the maintaining process. The demand for the GPU has increased rapidly recently due to the national regulations required to minimize the airport's air and noise pollution [1].

The inverter hardware system utilizes the three single-phase combined structure due to its benefits, especially in handling unbalanced loads. To eliminate switching frequency harmonics and isolate the fundamental voltage component, a simple LC filter is chosen over more complex filters. Additionally, the filter inductor is incorporated into the isolated transformer leakage, reducing system weight and magnetic core loss while enhancing power density. Fig. 1 illustrates the proposed design of the three-single-phase combined GPU.

Numerous control strategies for inverters have been explored in the literature [2–12]. Among them, traditional cascade control schemes based on inner current loops have been investigated [2–6]. These cascade control schemes have demonstrated their capability in delivering high voltage performance, particularly in the context of 50Hz industrial inverters. However, for high-power 400Hz inverters, where the output frequency is higher, there are limitations. The switching frequency is constrained for high-power switches, often unable to exceed 20kHz. This limitation results in a low ratio between the converter switching frequency and the fundamental frequency, constraining the control bandwidth. Consequently, adopting inner current loop control without complex predictive algorithms or time

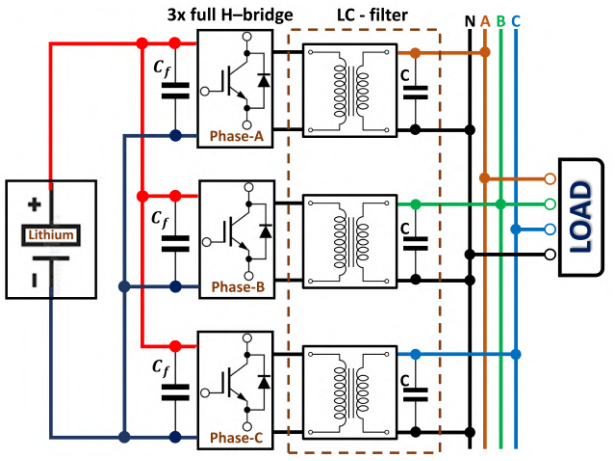

Fig. 1. Three single-phase combined GPU structure

delay compensation techniques becomes challenging. To circumvent the challenges associated with double-loop control, a single-loop control strategy emerges as a promising solution, as discussed in numerous publications. The synchronously rotating frame based single loop voltage control scheme is first examined for GPU in [7].

The experimental results demonstrate that the proposed control method can yield high-quality output voltage, even under nonlinear load conditions. However, the complex switching pattern poses constraints on practical design. In [8], a single loop resonant control is proposed for GPU to achieve zero steady-state error, and compensate the harmonic distortion. However, this control scheme may not provide as robust performance in handling disturbances and changes in the system. In [9], the repetitive control system based on Internal Model Principle has been used to minimize and eliminate the periodic errors. The slow dynamics, the high order of the controller are the major problems of this technique. To further improve the dynamic of closed-loop control system, the sliding mode control which advantages in robustness against external disturbances, and unpredictable parameter change has also been analyzed in [10–12]. Utilizing a time-varying sliding gain in the sliding function can enhance the dynamic performance of the control system [12]. Nevertheless, issues such as high-power loss due to variable switching frequency and chattering can still persist.

In the context of power converters, a disturbance observer is a vital element in control systems for estimating and compensating disturbances that can influence the system's performance. These observers are instrumental in addressing disturbances arising from factors like manufacturing tolerances, component aging, and load variations in power converters. To address these needs, various observer designs have been explored for application in inverters. More detail, [13–18] Luenberger and PI observers (PIobs) are designed to estimate the control variables.

Especially, in [17], the discrete PIobs has been developed to estimate the unknown disturbance, which enhances the accuracy of the calculation of the current setpoint. Nevertheless, for the proposed integrated transformer-inductor GPU structure, the inductance parameter is highly prone to change. Consequently, classical Luenberger or PIobs methods cannot ensure rapid convergence of the estimation errors to zero. Sliding mode observers have also been proposed for inverter systems in various publications [19–21].

These observers utilize a nonlinear switching term to incorporate the output estimation error, providing an attractive option dealing with unknown signals, model uncertainties, or nonlinear disturbances. Nonetheless, the control gain cannot be selected excessively high due to the practical constraint of the control surface deflection limit. Additionally, controlling chattering which leads to excessive control activity and can trigger high-frequency oscillations, is crucial in GPU practical applications. Reducing the switching gain has been a technique proposed to mitigate chattering [20]. However, this approach has resulted in increased steady-state errors in estimation. Adaptive observer can also provide the high accuracy estimated states by online adjusting the parameter to deal with system uncertainties and load changes [22]. But the slow estimation error convergence has restricted the observer performance.

The motivation of this article is to introduce a novel disturbance observer design specifically tailored for the proposed three single-phase combined GPU. This observer is intended to accurately estimate the output voltage, inductor current, and especially, system unmeasurable disturbances arising from variations in system parameters and changes in load. An observer-based single-loop digital control, focusing on preserving the inner inductor current rather than the typical direct output voltage, is then implemented for maintaining output voltage. In this control strategy, a setpoint current command generation technique is employed to achieve rapid tracking of the reference by the output voltage. The contributions of the article are summarized as follows.

1. A novel state and disturbance observer design based on the PR control algorithm is suggested for the 400Hz GPU, which aims to enhance the accuracy of state estimation and system disturbances, that cannot be physically measured by sensors. The design process of the PRobs is outlined in a detailed step-by-step manner as follows: Firstly, the system state space model, with

system disturbances included, is presented. The observability and controllability of the presented model, which are important aspects of state-variable analysis and design, are also demonstrated. Secondly, the methodology for designing the observer based on the PR control algorithm is analyzed. Finally, the convergence of the observer's state and disturbance estimation error is analytically proven. This study has also laid the fundamental for future work, where a higher order harmonic PR compensator will be integrated to compensate the harmonic disturbances induced by the nonlinear load.

2. A fully single loop digital control scheme which is based on PRobs is applied to manage the output voltage across different load conditions. The control scheme is aimed to compensate the estimated disturbances, maintain stable output voltage, consequently enhancing overall system dynamic performance.

This paper is organized as follows. Section 2 shows the system description. The PRobs is designed in Section 3. The control design with application of current setpoint generation technique is presented in Section 4. Matlab, real-time simulations and experiments in a variety of load scenarios are implemented in Section 5 to verify the proposed solution's performance. Finally, the conclusions are shown in Section 6.

2. System modeling

In the case of three single-phase combined topology, all the coupled terms between phases are significantly small that can be ignored, the continuous-time model of a three-phase GPU in Figure 1 can be treated as three single-phase circuits as shown in Fig. 2.

The state-space equations describing the operation of the inverter in continuous time domain are as follows [17]:

$$\begin{cases} \dot{x}(t) = Ax(t) + Bu(t) + d(t) \\ y(t) = Cx(t) \end{cases} \tag{1}$$

Where,

$$\begin{aligned} x(t) = y(t) &= \begin{bmatrix} v_o(t) \\ i_L(t) \end{bmatrix} \\ d(t) &= \begin{bmatrix} -R_C \frac{di_o(t)}{dt} - \frac{i_o(t)}{C_f} + d_1(t) \\ d_2(t) \end{bmatrix} \\ A &= \begin{bmatrix} -\frac{R_C}{L_f} & \left(\frac{1}{C_f} - \frac{R_C R_f}{L_f}\right) \\ -\frac{1}{L_f} & -\frac{R_f}{L_f} \end{bmatrix}, \\ B &= \begin{bmatrix} \frac{R_C V_d}{N L_f} \\ \frac{V_d}{N L_f} \end{bmatrix}, C = \begin{bmatrix} 1 & 0 \\ 0 & 1 \end{bmatrix} \end{aligned} \tag{2}$$

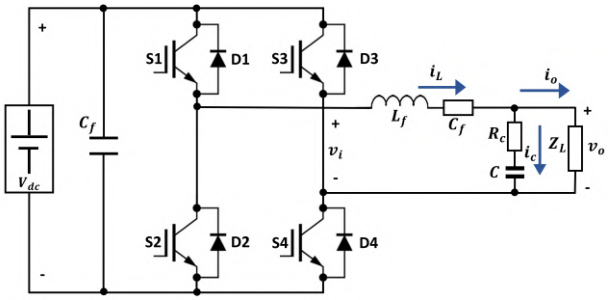

Fig. 2. Single phase inverter model

In Eq. (2), $i_L(t)$ and $i_o(t)$ are the inductor and the load current, R_f, R_C, L_f, C_f are the parameters of the equivalent LC filter, N is transformer ratio, $d_1(t), d_2(t)$ represent for the modeling errors can arise due to the variability of all parameters of the inverter during operation.

For control design purpose, a discrete time state-space model derived from Eq. (1) is used in this paper:

$$\begin{cases} X_{k+1} = \Phi X_k + \Gamma u_k + f_k \\ Y_k = C X_k \end{cases} \tag{3}$$

The corresponding state-space variables and matrices of the discrete-time system Eq. (3) are:

$$\begin{aligned} X_k = Y_k &= \begin{bmatrix} v_{o,k} \\ i_{L,k} \end{bmatrix}, \quad \Phi = e^{AT_s} = \begin{bmatrix} \phi_{11} & \phi_{12} \\ \phi_{21} & \phi_{22} \end{bmatrix} \\ \Gamma &= \int_0^{T_s} e^{A\tau} d\tau B = A^{-1}\left(\Phi - I_2\right) B = \begin{bmatrix} \Gamma_{11} \\ \Gamma_{21} \end{bmatrix} \\ f_k &= \int_0^{T_s} e^{A\tau} d\left\{(k+1)T_s - \tau\right\} d\tau = \begin{bmatrix} f_{1,k} \\ f_{2,k} \end{bmatrix} \end{aligned} \tag{4}$$

3. Pr observer design

This section is dedicated for presenting the design methodology of PR disturbance observer for GPU, with the model is expressed in Eq. (3).

3.1. System observability and controllability evaluation

The determinant of observability matrix and controllability matrix can be expressed:

$$|C_{ab}| = |B \quad AB| = -\frac{V_{dc}^2}{K^2 L_f^2 C_f} \neq 0 \tag{5}$$

$$|O_{ab}| = \begin{vmatrix} C \\ CA \end{vmatrix} = \frac{1}{L_f C_f} \neq 0 \tag{6}$$

It can be seen that C_{ab} and O_{ab} are not singular, so, system (3) is completely observable-controllable.

3.2. PR observer design

According to Assumptions in [13], if the sampling period T_s is sufficiently small, the disturbance $f(t)$ is smooth, it can be derived as:

$$\operatorname{rank}\left(\begin{bmatrix} \varphi - I_2 & I_2 \\ -C & 0 \end{bmatrix}\right) = 4 \tag{7}$$

And

$$\begin{cases} \lim_{T_s \to 0} |f_{k+1} - f_k| = 0 \\ \lim_{T_s \to 0} |f_{k+1} - 2f_k + f_{k-1}| = 0 \end{cases} \tag{8}$$

Which can be the foundation for designing the observer in the subsequent part.

The PRobs structure is depicted in Fig. 3 below. The s domain transfer function of the observer is as follow:

$$\frac{f_{(s)}}{e_{(s)}} = \frac{K_r s}{s^2 + \omega_0^2} \tag{9}$$

By using Forward Euler, we get the discrete function of observer:

$$\begin{aligned} \frac{e_k}{f_k} &= \frac{K_r \left(\frac{z-1}{T_s}\right)}{\left(\frac{z-1}{T_s}\right)^2 + \omega_0^2} \\ &= \frac{K_r T_s \left(z^{-1} - z^{-2}\right)}{1 - 2z^{-1} + \left(1 + T_s^2 \omega_0^2\right) z^{-2}} \end{aligned} \tag{10}$$

which can be rewritten:

$$f_k - 2f_{k-1} + \left(1 + T_s^2 \omega_0^2\right) f_{k-2} = K_r T_s \left(e_{k-1} - e_{k-2}\right) \tag{11}$$

If we define $\hat{X}_k$ and $\hat{f}_k$ as the estimation state and the estimation disturbance, $\tilde{X}_k$ and $\tilde{f}_k$, which means:

$$\begin{aligned} \tilde{X}_k &= X_k - \hat{X}_k \\ \tilde{Y}_k &= Y_k - \hat{Y}_k \\ \tilde{f}_k &= f_k - \hat{f}_k \end{aligned} \tag{12}$$

The state space Eq. (3) can be transformed to discrete PRobs as follows:

$$\begin{cases} \hat{X}_{k+1} = \Phi \hat{X}_k + \Gamma u_k + L_1 \left(Y_k - \hat{Y}_k\right) + \hat{f}_k \\ \hat{f}_{k+1} = 2\hat{f}_k - \left(1 + T_s^2 \omega_0^2\right) \hat{f}_{k-1} + K_r T_s \left(\tilde{Y}_k - \tilde{Y}_{k-1}\right) \\ \hat{Y}_k = C \hat{X}_k \end{cases} \tag{13}$$

3.3. PR observer convergence analysis

From Eq. (3) and Eq. (13) we have:

$$\tilde{X}_{k+1} = (\Phi - L_1 C) \tilde{X}_k + \tilde{f}_k \tag{14}$$

with $\tilde{f}_k = f_k - \hat{f}_k$, we get:

$$\begin{aligned} &\tilde{f}_{k+1} = f_{k+1} - \hat{f}_{k+1} \\ &= (f_{k+1} - f_k) + \left(f_k - \hat{f}_k\right) + \left(\hat{f}_k - \hat{f}_{k+1}\right) \\ &= (f_{k+1} - f_k) + \tilde{f}_k - \hat{f}_k \\ &+ \left(1 + T_s^2 \omega_0^2\right) \hat{f}_{k-1} - K_r T_s \left(\tilde{X}_k - \tilde{X}_{k-1}\right) \\ &= -K_r T_s \tilde{X}_k + 2\tilde{f}_k \\ &+ \left[f_{k+1} - 2f_k + \left(1 + T_s^2 \omega_0^2\right) \hat{f}_{k-1} + K_r T_s \tilde{X}_{k-1}\right] \end{aligned} \tag{15}$$

Finally, the state space estimation equation can be obtained:

$$\begin{aligned} &\begin{bmatrix} \tilde{X}_{k+1} \\ \tilde{f}_{k+1} \end{bmatrix} = \begin{bmatrix} \Phi - L_1 C & I_2 \\ -L_2 C & 2I_2 \end{bmatrix} \begin{bmatrix} \tilde{X}_k \\ \tilde{f}_k \end{bmatrix} \\ &+ \begin{bmatrix} 0 \\ f_{k+1} - 2f_k + \left(1 + T_s^2 \omega_0^2\right) \hat{f}_{k+1} + L_2 \tilde{Y}_{k-1} \end{bmatrix} \\ &= (M - LG) \begin{bmatrix} \tilde{X}_k \\ \tilde{f}_k \end{bmatrix} + O\left(T_s\right) \end{aligned} \tag{16}$$

Where,

$M = \begin{bmatrix} \Phi & I_2 \\ 0 & 2I_2 \end{bmatrix}, L = \begin{bmatrix} L_1^T & L_2^T \end{bmatrix}, G = \begin{bmatrix} C & 0 \end{bmatrix}$

And $O\left(T_s\right)$ means exponent of number of T_s .

With the Assumption 1 in Eq. (5) is satisfied, according to [13], it can be derived from Eq. (16) as:

$$\begin{cases} \lim\limits_{k \to \infty} \left(X_k - \hat{X}_k\right) = O\left(T_s\right) \\ \lim\limits_{k \to \infty} \left(f_k - \hat{f}_k\right) = O\left(T_s\right) \end{cases} \tag{17}$$

Which demonstrate that the estimation error can be converged to a small value O(T_s). The observer matrix gain L, which decide the convergence time, can be determined using pole placement method. Normally, L is designed so that the eigenvalues of (M-LG) is close to the origin of the unit circle to reduce the observer response time.

4. Design of output voltage control system

4.1. Current command generator

The state space model Eq. (3) can be rewritten:

$$V_{o,k+1} = \phi_{11} V_{o,k} + \phi_{12} I_{L,k} + \Gamma_{11} u_k + f_{1,k} \tag{18}$$

$$I_{L,k+1} = \phi_{21} V_{o,k} + \phi_{22} I_{L,k} + \Gamma_{21} u_k + f_{2,k} \tag{19}$$

To keep the output voltage $V_{o,k}$ follows a desired voltage $V_{o,k}^*$, an appropriate reference inductor current $I_{L,k+1}^*$ is needed for the current loop [17], the process for generating $I_{L,k+1}^*$ is as follow.

First, the voltage tracking error $E_{v,k}$ is defined:

$$E_{v,k} = e_{v,k} - \lambda e_{v,k-1} \tag{20}$$

where $0 < \lambda < 1$ is a design parameter, and $e_{v,k}$ is the instantaneous voltage tracking error computed by:

$$e_{v,k} = V^*_{o,k} - V_{o,k} \tag{21}$$

Base on Eqs. (20) and (21), $E_{v,k}$ can be expressed as:

$$\begin{aligned} E_{v,k+1} &= e_{v,k+1} - \lambda e_{v,k} \\ &= V^*_{o,k+1} - V_{o,k+1} - \lambda \left(V^*_{o,k} - V_{o,k} \right) \end{aligned} \tag{22}$$

From Eqs. (18) and (19) and Eq. (22), $E_{v,k}$ can be extended:

$$\begin{aligned} E_{v,k+1} = V^*_{o,k+1} - \lambda V^*_{o,k} + \left(\frac{\Gamma_{11}}{\Gamma_{21}} \phi_{21} - \phi_{11} + \lambda \right) V_{o,k} \\ + \left(\frac{\Gamma_{11}}{\Gamma_{21}} \phi_{22} - \phi_{12} \right) I_{L,k} + \frac{\Gamma_{11}}{\Gamma_{21}} f_{2,k} - f_{1,k} - \frac{\Gamma_{11}}{\Gamma_{21}} I_{L,k+1} \end{aligned} \tag{23}$$

To force $e_{i,k+1}$, the one step-ahead current tracking error, the control signal u_k can be found as a solution of the equation:

$$e_{i,k+1} = I^*_{L,k+1} - I_{L,k+1} = 0 \tag{24}$$

Since $f_{1,k}$ and $f_{2,k}$, k are unknowns, these approximations are employed:

$$\begin{cases} f_{1,k} \approx \hat{f}_{1,k} \\ f_{2,k} \approx \hat{f}_{2,k} \end{cases} \tag{25}$$

To make $E_{v,k+1} = 0$ the reference current equation can be expressed:

$$\begin{aligned} I^*_{L,k+1} = \frac{\Gamma_{21}}{\Gamma_{11}} \left(V^*_{o,k+1} - \lambda V^*_{o,k} \right) + \left(\phi_{22} - \frac{\Gamma_{21}}{\Gamma_{11}} \phi_{12} \right) I_{L,k} \\ + \left[\phi_{21} - \frac{\Gamma_{21}}{\Gamma_{11}} \left(\phi_{11} - \lambda \right) \right] V_{o,k} + \hat{f}_{2,k} - \frac{\Gamma_{21}}{\Gamma_{11}} \hat{f}_{1,k} \end{aligned} \tag{26}$$

The analysis of the voltage tracking error dynamic is similar to the aforementioned current control-loop. In details, substitutes Eq. (26) into Eq. (24), it results in

$$E_{v,k+1} = \frac{\Gamma_{21}}{\Gamma_{11}} \left(f_{2,k} - \hat{f}_{2,k} \right) - \left(f_{1,k} - \hat{f}_{1,k} \right) = O\left(T_s\right) \tag{27}$$

Then, substitute Eq. (27) into Eq. (20), it gives

$$\begin{aligned} e_{v,k} = \lambda^k e_{v,o} \\ + \sum_{i=0}^{k-1} \lambda^i O\left(T_s\right) = \lambda^k e_{v,o} + O\left(T_s\right) \frac{\lambda^k - 1}{\lambda - 1} \end{aligned} \tag{28}$$

in which, $e_{v,o}$ is the initial tracking error. Since $0 < \lambda < 1$, it can be concluded that:

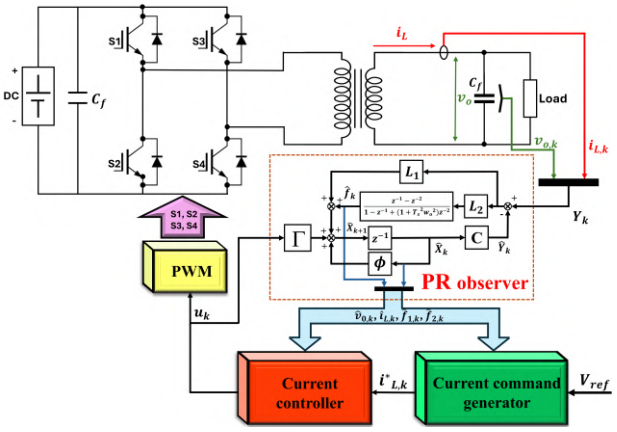

Fig. 3. Proposed PR observer-based control system scheme

$$\lim_{k \to \infty} e_{v,k} = O\left(T_s\right) \frac{1}{\lambda - 1} = O\left(T_s\right) \tag{29}$$

4.2. Controller design

Combine Eq. (19) and Eq. (24) fundamental equation for control signal yields [17]:

$$u_k = \frac{1}{\Gamma_{21}} \left(I^*_{L,k+1} - \phi_{21} V_{o,k} - \phi_{22} I_{L,k} - f_{2,k} \right) \tag{30}$$

The control action for the current loop is then:

$$u_k = \frac{1}{\Gamma_{21}} \left(I^*_{L,k+1} - \phi_{21} V_{o,k} - \phi_{22} I_{L,k} - \hat{f}_{2,k} \right) \tag{31}$$

The stability of the current-loop controller can easily be evaluated through $e_{i,k+1}$ as following:

$$e_{i,k+1} = I^*_{L,k+1} - \left[\phi_{21} V_{o,k} + \phi_{22} I_{L,k} + \Gamma_{21} u_k + f_{2,k} \right] \tag{32}$$

It can be rewritten that:

$$e_{i,k+1} = f_{2,k} - \hat{f}_{2,k} = O\left(T_s\right) \tag{33}$$

which indicates that when the poles of the observer are accurately selected to ensure rapid convergence of $\hat{f}_{2,k}$ to $f_{2,k}$, the tracking error $e_{i,k+1}$ approaches $O\left(T_s\right)$ after one step.

5. Simulation and experiment results

5.1. System parameter

The design parameters of the inverter, and control system are listed in Table 1.

Table 1. The system parameters

Parameter	Value
Rated output voltage	170 V
DC bus voltage	300 V
Filter inductance	200mH
Inductance resistance	0.2Ω
Filter capacitance	25μF
PWM frequency	18kHz
Sampling frequency	18kHz
Pole locations	$[0,05 \quad 0,1 \quad 0,15 \quad 0,023]$
L_1	$\begin{bmatrix} 1,7515 & 1,0679 \\ -0,1335 & 1,7478 \end{bmatrix}$
$\boldsymbol{L}_2$	$\begin{bmatrix} 0,8304 & 0 \\ 0 & 0,8550 \end{bmatrix}$

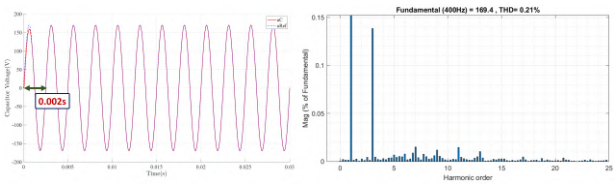

Fig. 4. Output voltage and THD for the linear load situation

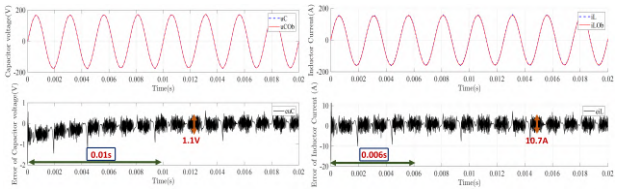

Fig. 5. The estimated voltage and current, and the estimated error in the linear load condition

5.2. Simulation

MATLAB Simulations The initial simulation focuses on a resistive load scenario. As depicted in Fig. 4, the output voltage swiftly stabilizes at the reference value within approximately 0.002 seconds, exhibiting almost perfect regulation and indicating an almost negligible steadystate error. Additionally, the Total Harmonic Distortion (THD) content is merely 0.21%. For the observer response, it is demonstrated in Fig. 5a) an outstanding performance in estimating the output voltage, with the error is restricted at 1 V peak-to-peak.

Typically, the inductor current estimation error is higher than that of voltage due to the characteristics of inductors, as expressed in Fig. 5b), where the current estimation error is higher at around 10V peak-to-peak, even including some high notches corresponding to the current peaks. Due to the magnetic field stored, rapid changes in current can induce voltage spikes affecting the accurate estimation of the current, increasing the estimation error. Normally, the performance of the inductor current estimation is dependent on the pole placement. The location of the poles in this research are determined in an experience-based manner, which are closed to the origin of the unit circle. To improve, optimization techniques can be applied for further research to find optimal pole locations improving system performance.

Next, the performance of the control system under underloaded conditions is evaluated, with the load set to 50% and 70% between 0.01s to 0.02s and 0.03s to 0.04s, respectively. Analysis of the results in Fig. 6a) reveals minimal deviation in the output voltage waveform, with both magnitude and phase of the steady-state error remaining small, even during load variations. The current quickly returns to its normal state after the load change.

In contrast, when comparing with the PIobs method, as shown in Fig. 7a), there is an observable phase delay of 8° in the output voltage with respect to the reference, adversely affecting system performance. In the steady state, the voltage estimation error is nearly zero, and during transients, it rises to just 1.8V, as depicted in Fig. 6b), demonstrating significant improvement compared to the PIobs method illustrated in Fig. 7b).

The dynamic response of the proposed control system and the effectiveness of the PRobs compared to the traditional PIobs in handling nonlinear loads are further investigated. Additionally, single loop PR control strategy is simulated for comparative purposes. Fig. 8a) displays the output voltage and current waveforms with minimal distortions. Despite the nonlinear load with the crest factor is 1.68, the output voltage THD remains low at 2.26%. This performance surpasses that of the PIobs, with THD is 2.45% (Fig. 8b)), and of the single loop PR control strategy case, where the THD is 3.34% (Fig. 8c)). This result highlights the superiority of PRobs over traditional PIobs [17]

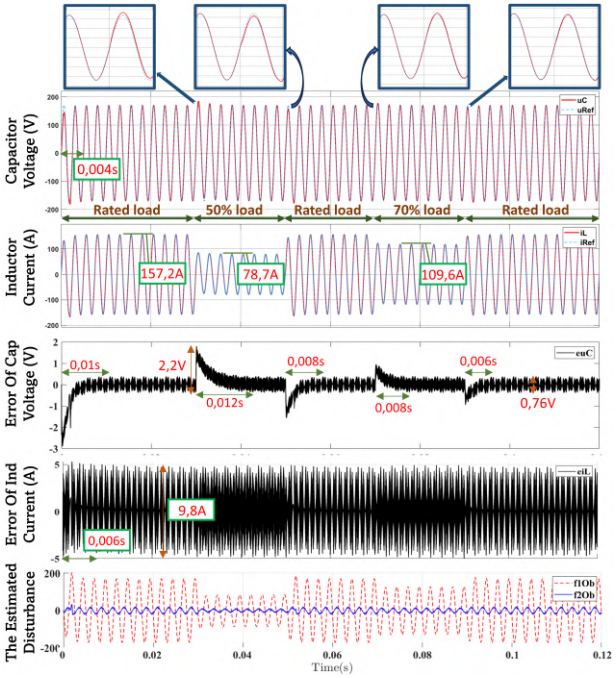

Fig. 6. The proposed system response under load change conditions a) Voltage and current waveform, b) Voltage estimation error, c) Current estimation error, d) Estimated f1 and f2 disturbances

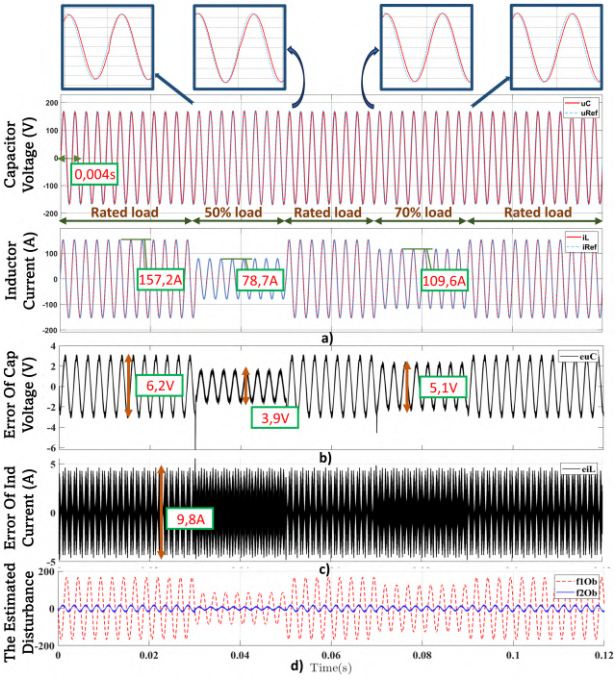

Fig. 7. The system response under load change conditions with the PIobs a) Voltage and current waveform, b) Voltage estimation error, c) Current estimation error, d) Estimated f1 and f2 disturbances

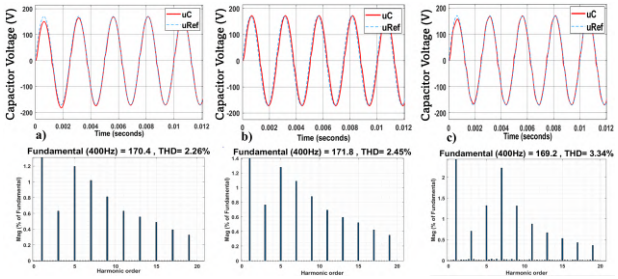

Fig. 8. a) Proposed controller, b) Single loop PR controller, c) PIob instead

in mitigating the impact of AC disturbances, as described in Eq. (26), even when only a fundamental PR controller is employed. The performance of the PRobs estimation, and consequently the control system, is anticipated to see further significant enhancements in handling nonlinear loads in future work, with the incorporation of higher-order harmonic controllers.

In the final assessment, the robustness of the proposed control system is showcased under conditions of system parameter variations and nonlinear load, maintaining a crest factor of 1.68 as in the previous scenario. A simulation scenario is constructed where both the filter capacitor and filter inductor are increased by 20%. The simulation results in Fig. 9a) illustrate that the novel control approach continues to deliver a high-quality output voltage, with a THD of just 2.17%. Conversely, when the PRobs is replaced by PIobs, as shown in Fig. 9b), the output voltage exhibits lower quality with phase delay, resulting in a higher THD of 2.35%. Additionally, Fig. 9c) displays the result of the single loop PR control case, indicating more pronounced distortions in the output voltage waveform, particularly in the zero-crossing region, with a relatively high THD of 3.23%. These findings underscore the effectiveness of the proposed control strategy based on the PRobs. Particularly noteworthy is its performance under conditions of system parameter changes, where the disturbance f1 affects the system. The PR algorithm, whose gain is finite at fundamental frequency 400Hz, successfully eliminates steady-state estimation errors and provides highly accurate estimations of voltage, current, and disturbance. Consequently, the response of the control system is significantly enhanced compared to PIobs or single loop PR control approaches.

The estimated disturbances f1 and f2 are observable, as depicted in Fig. 10. As can be described in state space Eq. (3), f1 and f2 are mappings of disturbances d1 and d2 in the discrete domain, fundamentally representing the deviation in the derivative of state variables, specifically, the inductor current and the output voltage across the capaci-

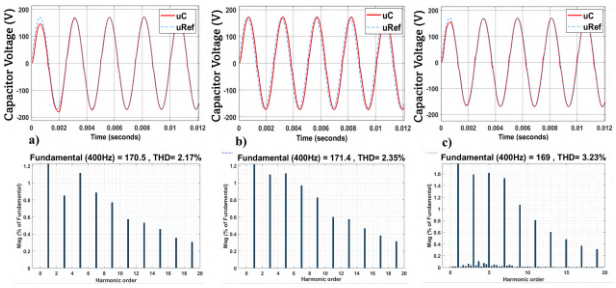

Fig. 9. The output voltage and THD under system parameter change condition a) Proposed controller, b) Single loop PR controller, c) PIob instead

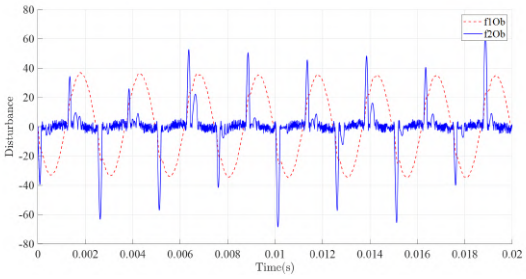

Fig. 10. The estimated disturbances under parameter change condition

tor.

HIL Simulations The GPU system under consideration is tested using a real-time system by implementing it on the Hardware-in-Loop (HIL) device. The actual HIL simulation setup can be seen in Fig. 11.

The control system is initially assessed using a linear load. The output waveform is regulated to the reference value with minimal deviation, resulting in a THD of only 1.18%, as shown in Fig. 12. The accurate estimation of the output voltage and inductor current depicted in Figure 13 showcases the effectiveness of the PRobs.

The proposed control system is then investigated under load change conditions, where the load shifts from being underloaded by 50% in 0.01 seconds to fully loaded in another 0.01 seconds. Figures 14 and 15 display the swift recovery of the output voltage and inductor current during this load transition. Despite the significant load change, the output voltage THD remains at an acceptable level of 3.89%.

Finally, the system performance under nonlinear load has been checked. The advantages of the PRobs especially in the case of harmonic distortion caused by nonlinear load are verified by contrasting to the case of PIobs.

As depicted in Fig. 16, the output voltage quality has decreased due to the influence of nonlinear load, resulting in

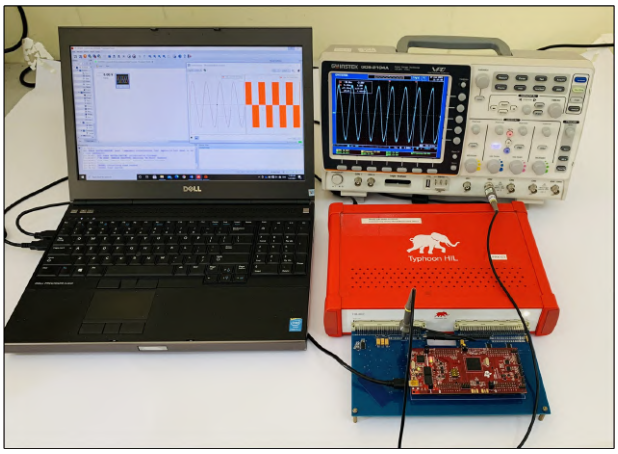

Fig. 11. HIL real time simulation system

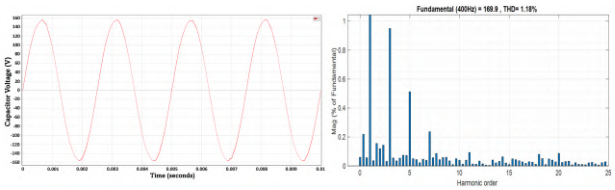

Fig. 12. Output voltage and THD with linear load

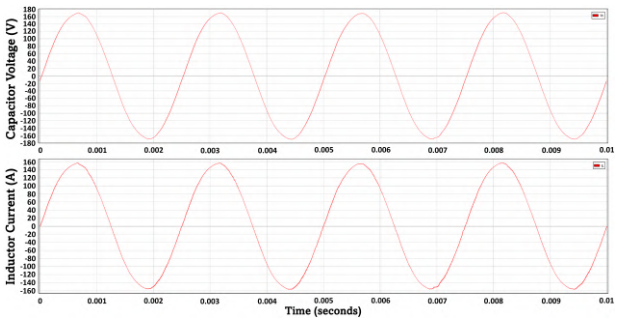

Fig. 13. Estimated voltage and current under linear load condition

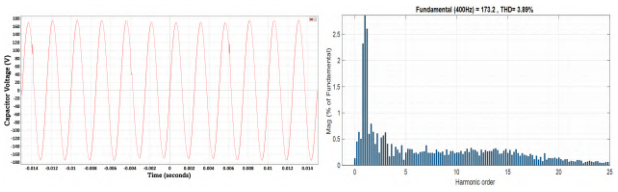

Fig. 14. Output voltage under load change condition

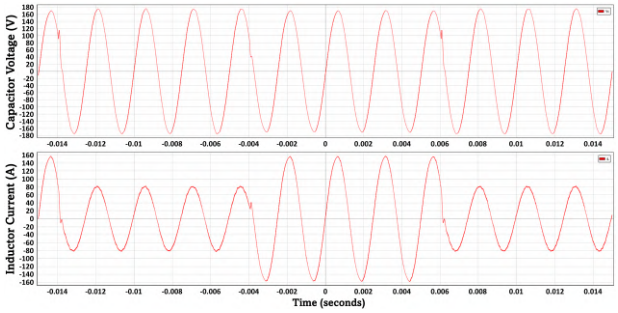

Fig. 15. Estimated voltage and current under load change condition

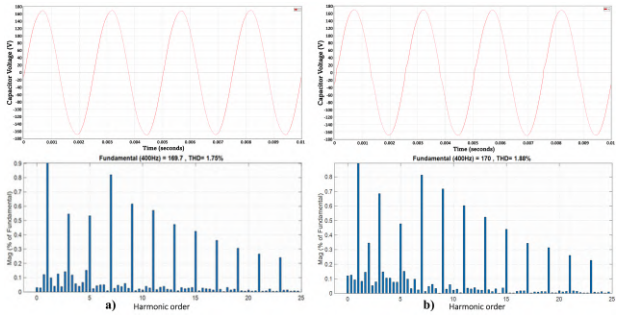

Fig. 16. Output voltage under nonlinear load condition a) PRobs b) PIobs

an increase in the Total Harmonic Distortion (THD) content from 1.18% under linear load conditions to 1.75%. However, this value remains lower than when PIobs is applied, indicating the superior response of the proposed PRobs in nonlinear load operations.

5.3. Experimental Setups

To validate the proposed sliding mode observer-based control scheme, a DSP-controlled PWM inverter was implemented. The main processor of the digital control system was a Texas Instruments Inc. microprocessor, specifically the TMS320F28035. Four IGBTs with the model number FGH60N60 were chosen as the power switches.

The initial experiment is conducted under no-load conditions. It is observed that the output waveform closely resembles a perfect sinusoid. The error in both the frequency and magnitude of the output voltage is negligible. The THD content, depicted in Fig. 18, is only 2.13

Fig. 19 presents the experimental result of the output voltage under a resistive load transitioning from no load to full load. The voltage drop occurring at the moment of load variation is quickly recovered by the designed digital controller within 0.025s. Moreover, the THD remains consistently at 1.17%, showcasing the effectiveness of the proposed control method.

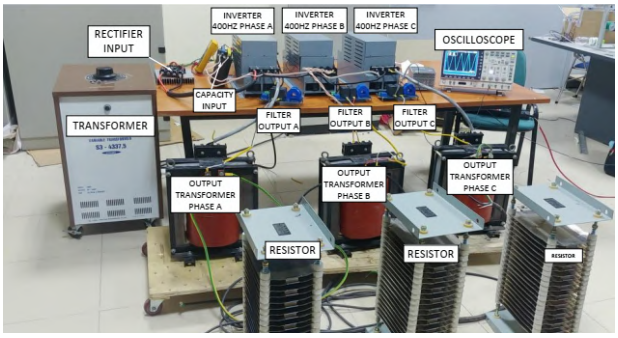

Fig. 17. Experiment system

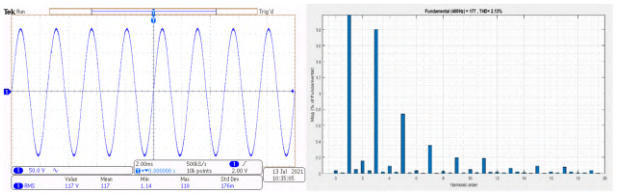

Fig. 18. No load condition output voltage and THD

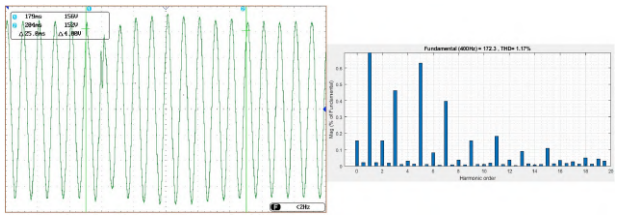

Fig. 19. No load to full resistive load switching condition

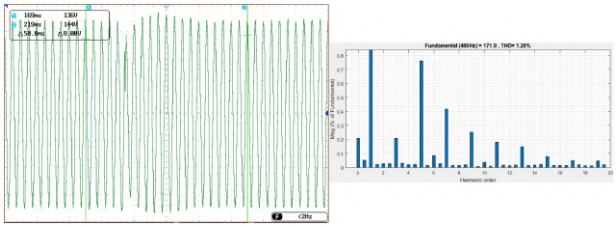

Fig. 20. Overload 150% output voltage and THD content

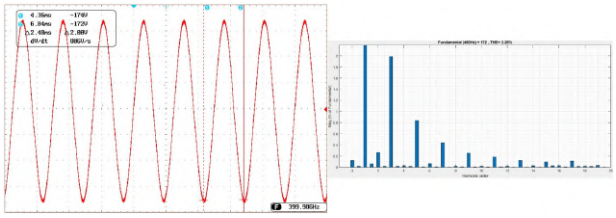

Fig. 21. Output voltage and THD under nonlinear load condition

The control system dynamics are further examined under overload conditions. Fig. 20 illustrates the output voltage under a resistive load transitioning from no load to 150% overload. It is evident from the experimental results that the output voltage swiftly returns to a stable value within just 0.025 seconds. Additionally, the THD content remains low, at just 1.2%.

Finally, the experimental waveform under a rectifier load with a current crest factor of 3.4 is performed. THD content of the output voltage was measured at 2.38% as shown in Fig. 21. Despite the connection of a highly nonlinear load, the sinusoidal output waveform could still be preserved, highlighting the significant contribution of the proposed PRobs and the control system design.

6. Conclusions

This paper presents a novel design of a Proportional Resonant observer (PRobs) for 400Hz GPU, aimed at estimating states, particularly output voltage and inductor current, while addressing disturbances stemming from system parameter tolerances, variations, and load changes. Theoretical analysis of the PRobs has been carried out which illustrates its capability to provide robust estimation responses in handling AC disturbances. Additionally, an PRobs-based single-loop digital control strategy for the inverter system is applied to regulate the output voltage under various load conditions. Both MATLAB simulations and Hardware-in-the-Loop (HIL) simulations, along with experimental results, demonstrate the effectiveness of the proposed PRobs, consequently, the overall control system.

References

[1] J. Xie, L. Zhu, and H. M. Lee, (2023) *"Aircraft noise reduction strategies and analysis of the effects"* **International Journal of Environmental Research and Public Health *20***(2): 1352. DOI: 10.3390/ijerph20021352.

[2] J. Zhu, Z. Nie, W. Ma, and S. Nie. "Comparison between DB control and dual-loop PR control for collapsed H-bridge single-phase 400Hz power supply". In: *2012 IEEE International Symposium on Industrial Electronics*. IEEE. 2012, 240–245. DOI: 10.1109/ISIE.2012.6237091.

[3] D. Manohar and P. Seema. "Deadbeat controller with phase corrector for 400-Hz inverter used in ground power units of aircrafts". In: *2015 International Conference on Technological Advancements in Power and Energy (TAP Energy)*. IEEE. 2015, 127–131. DOI: 10.1109/TAPENERGY.2015.7229604.

[4] S. Mudaliyar, D. Pullaguram, S. Mishra, and N. Senroy. "Cascaded fractional order and sliding mode control for an autonomous voltage source inverter". In: *2018 IEEE Power & Energy Society General Meeting (PESGM)*. IEEE. 2018, 1–5. DOI: 10.1109/PESGM.2018.8585985.

[5] F. Rojas, R. Cardenas, J. Clare, M. Diaz, J. Pereda, and R. Kennel, (2019) *"A design methodology of multiresonant controllers for high performance 400 Hz ground power units"* **IEEE Transactions on Industrial Electronics *66***(8): 6549–6559. DOI: 10.1109/TIE.2019.2898610.

[6] W. Yao, J. Cui, and W. Yao, (2020) *"Single-phase inverter deadbeat control with one-carrier-period lag"* **Electronics *9***(1): 154. DOI: doi.org/10.3390/electronics9010154.

[7] M. Monfared, S. Golestan, and J. M. Guerrero, (2013) *"Analysis, design, and experimental verification of a synchronous reference frame voltage control for single-phase inverters"* **iEEE Transactions on industrial Electronics *61***(1): 258–269.

[8] Z. Li, Y. Li, P. Wang, H. Zhu, C. Liu, and F. Gao, (2009) *"Single-loop digital control of high-power 400-Hz ground power unit for airplanes"* **IEEE transactions on industrial electronics *57***(2): 532–543. DOI: 10.1109/TIE.2009.2033490.

[9] W. M. Rohouma, S. L. Arevalo, P. Zanchetta, and P. Wheeler, (2010) *"Repetitive control for a four leg matrix converter"*:

[10] S. Chiang, T. Tai, and T. Lee, (1998) *"Variable structure control of UPS inverters"* **IEE Proceedings-Electric Power Applications *145***(6): 559–567.

[11] O. Kukrer, H. Komurcugil, and A. Doganalp, (2009) *"A three-level hysteresis function approach to the sliding-mode control of single-phase UPS inverters"* **IEEE Transactions on Industrial Electronics *56***(9): 3477–3486.

[12] H. Komurcugil, (2011) *"Rotating-sliding-line-based sliding-mode control for single-phase UPS inverters"* **IEEE Transactions on Industrial Electronics *59***(10): 3719–3726.

[13] J.-W. Kho, J.-Y. Jang, and K.-B. Lee. "Disturbance observer-based deadbeat control for single-phase UPS inverters". In: *SICE 2003 Annual Conference (IEEE Cat. No. 03TH8734)*. **2**. IEEE. 2003, 1206–1210.

[14] J.-L. Chang, (2006) *"Applying discrete-time proportional integral observers for state and disturbance estimations"* **IEEE Transactions on Automatic Control *51***(5): 814–818. DOI: 10.1109/TAC.2006.875019.

[15] M. Xue, Y. Zhang, F. Liu, Y. Kang, and Y. Yi. "Optimized pole and zero placement with state observer for LCL-type grid-connected inverter". In: *2011 IEEE Energy Conversion Congress and Exposition*. IEEE. 2011, 377–382. DOI: 10.1109/ECCE.2011.6063794.

[16] M. Wang, Y. Xu, and J. Zou, (2020) *"Sliding mode control with open-switch fault diagnosis and sensorless estimation based on PI observer for PMSM drive connected with an LC filter"* **IET Power Electronics *13***(11): 2334–2341. DOI: 10.1049/iet-pel.2019.1233.

[17] M. L. Nguyen and P. Vu, (2021) *"Advanced single-loop discrete-time control for T-type voltage source inverter-with minimum capacitor voltage ripple modulation"* **Turkish Journal of Electrical Engineering and Computer Sciences *29***(7): 2962–2982.

[18] A. Hadjkaddour, O. Bouchhida, H. Benguesmia, A. Chouder, A. Cherifi, and M. Saoudi. "DeadBeat Controller Based Luenberger Current Observer for Single-phase Islanded Inverter". In: *2022 19th International Multi-Conference on Systems, Signals & Devices (SSD)*. IEEE. 2022, 1461–1465. DOI: 10.1109/SSD54932.2022.9955497.

[19] G.-X. Zhong, Z. Wang, J. Li, and Q. Su, (2023) *"Robust fault diagnosis for closed-loop grid-connected inverter based on sliding mode observer and identifier"* **Electric Power Systems Research *217***: 109097. DOI: 10.1016/j.epsr.2022.109097.

[20] A. T. Duong, T. L. Pham, P. Vu, et al., (2023) *"Disturbance Observer Based on Fixed Time Sliding Mode Control and Optimal State Observer for Three-Phase Three-Level T-type Inverters"* **IEEE Access**: DOI: 10.1109/ACCESS.2023.3281672.

[21] J. Huang, F. Ding, and Y. Wang. "Sliding mode control with nonlinear disturbance observer for a class of underactuated system". In: *Proceedings of the 32nd Chinese Control Conference*. IEEE. 2013, 541–546.

[22] X. Xu, S. Vazquez, H. Luo, L. G. Franquelo, and E. Zafra. "Data-driven Adaptive Observer-based Predictive Control for an Inverter with Output LC Filter". In: *IECON 2022–48th Annual Conference of the IEEE Industrial Electronics Society*. IEEE. 2022, 1–6. DOI: 10.1109/IECON49645.2022.9969052.